Journal of Alloys and Compounds 495 (2010) 167–172

Contents lists available at ScienceDirect

Journal of Alloys and Compounds

journal homepage: www.elsevier.com/locate/jallcom

Influence of non-isovalent ion substitution at A site on microstructure and magnetic properties of $Ba(Ti_{0.3}Fe_{0.7})O_3$ ceramic

Fangting Lin, Wangzhou Shi*

Key Laboratory of Optoelectronic Material and Device, and Department of Physics, Shanghai Normal University, Shanghai 200234, PR China

ARTICLE INFO

Article history:
Received 13 August 2009
Received in revised form 13 January 2010
Accepted 20 January 2010
Available online 1 February 2010

Keywords:
Ferroelectrics
Solid-state reactions
Microstructure
Magnetic measurements
Mössbauer spectroscopy

ABSTRACT

The $(Ba_{0.8}K_{0.2})(Ti_{0.3}Fe_{0.7})O_3$ ceramic was prepared by solid-state reaction, and post-annealed in oxygen ambient. By comparison with $Ba(Ti_{0.3}Fe_{0.7})O_3$ made under identical conditions, the effect of non-isovalent A-site substitution of K^+ on microstructure and magnetism of as-prepared and annealed $Ba(Ti_{0.3}Fe_{0.7})O_3$ samples was investigated using X-ray diffraction, Mössbauer spectroscopy, vibrating sample magnetometer and iodometric titration. It is found that all samples have a single 6H-$BaTiO_3$-type hexagonal perovskite structure without any impurities detected, regardless of A-site K^+ substitution or annealing. In the as-prepared state, non-isovalent A-site substitution of K^+ induces the variation in Fe occupational site, resulting in the disappearance of room-temperature ferromagnetism. The super-exchange interactions of Fe^{3+} at tetrahedral and octahedral Ti sites determine the paramagnetism of $(Ba_{0.8}K_{0.2})(Ti_{0.3}Fe_{0.7})O_3$. During the O_2 annealing process, the presence of Fe^{4+}, an unusual valence for iron, besides Fe^{3+} is observed, both distributed over octahedral Ti site. By A-site substitution of K^+ with a lower valence than Ba^{2+}, the charge compensation mechanism is further enhanced, and thus more Fe^{3+} ions are oxidized to Fe^{4+} in annealed $(Ba_{0.8}K_{0.2})(Ti_{0.3}Fe_{0.7})O_3$. Consequently, the ferromagnetic Fe^{4+}–O^{2-}–Fe^{4+} super-exchange interactions are strengthened, which leads not only to a paramagnetism–ferromagnetism transition but also to a higher saturation magnetization compared with annealed $Ba(Ti_{0.3}Fe_{0.7})O_3$.

1. Introduction

Achieving ferromagnetic ordering in ferroelectrics through impurity doping has become one of the most promising directions for multiferroic research [1–10]. Multiferroic materials are quite rare in nature, particularly at room temperature and above. In these compounds, electric and magnetic orders coexist, with some couplings between them (the magnetoelectric effect) [11], providing an additional degree of freedom in device design. Therefore, multiferroics have been the subject of intensive investigations due to their potential applications in the emerging field of spintronics [12], data-storage media [13], multiple-state memories [14], etc. Being an important ferroelectric material, $BaTiO_3$ is widely used in capacitors, positive temperature coefficient of resistance thermistors, chemical sensors and piezoelectric devices. Meanwhile, the ABO_3-type perovskite structure of $BaTiO_3$ determines its ability to accommodate a wide variety of cations at both the A and B sites, which offers the potential of possessing a very high degree of flexibility on composition, structure and properties. Hence the relevant work on ferromagnetism of $BaTiO_3$ doped with 3*d* transition metal has been reported theoretically [1] and experimentally [2–5].

So far almost all research on magnetism of doped $BaTiO_3$ has been focused on B-site substitution. In our previous work, room-temperature ferromagnetism was realized in $Ba(Ti_{1-x}Fe_x)O_3$ ceramics also by partial Fe substitution at the B site [15]. Then the magnetization was remarkably enhanced via subsequent O_2 annealing due to the ferromagnetic Fe^{4+}–O^{2-}–Fe^{4+} couplings produced by the presence of Fe^{4+} [16]. Moreover, other transition metals were codoped with Fe at the B site to induce new magnetic exchange mechanisms between ions with different valence states and occupational sites, giving rise to a further improvement of magnetic properties [17]. However, no work referring to A-site substitution has been reported up to now, among research on magnetism of transition-metal-doped $BaTiO_3$ system.

In the perovskite structure, the replacement of Ti^{4+} by Fe^{3+} implies the formation of one oxygen vacancy for two pentahedral Ti sites or one tetrahedral Ti site [18,19]. Considering the ABO_3 structure characteristics, further non-isovalent substitution of an ion, with a lower valance than Ba^{2+}, at the A site of $Ba(Ti_{1-x}Fe_x)O_3$ will facilitate the formation of oxygen vacancies in order to keep charge balance. Accordingly, the distribution of Fe occupational sites will be changed among octahedral, pentahedral and tetrahedral Ti sites, leading to various magnetic exchange mechanisms and magnetic properties. Furthermore, combining such non-isovalent A-site substitution with O_2 annealing can be expected to enable more Fe^{3+} ions to be oxidized to Fe^{4+}. As a result, the ferromagnetic

* Corresponding author. Tel.: +86 21 64328895.
E-mail address: nounou7@163.com (W. Shi).

0925-8388/$ – see front matter © 2010 Elsevier B.V. All rights reserved.
doi:10.1016/j.jallcom.2010.01.113

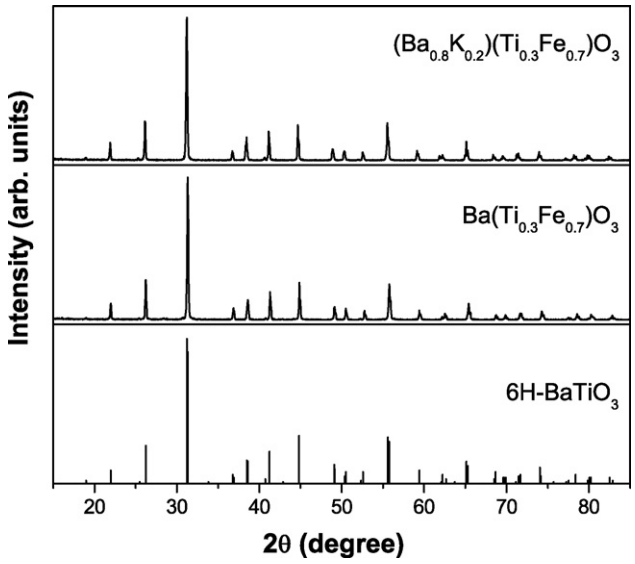

Fig. 1. XRD patterns of $(Ba_{0.8}K_{0.2})(Ti_{0.3}Fe_{0.7})O_3$ and $Ba(Ti_{0.3}Fe_{0.7})O_3$ ceramics.

Fe^{4+}–O^{2-}–Fe^{4+} couplings will be enhanced, and so will the magnetization. These are the primary work of the present article. Here, K^+ was selected to substitute for the A-site ion, based on its lower valence and almost the same size [20] compared with Ba^{2+}.

2. Experimental

High-purity (above 99.9%) carbonate and oxide powders were used to prepare $(Ba_{0.8}K_{0.2})(Ti_{0.3}Fe_{0.7})O_3$ by conventional ceramic technique. For comparison, $Ba(Ti_{0.3}Fe_{0.7})O_3$ was also synthesized under identical conditions. The doping site of K and Fe ions in $BaTiO_3$ was controlled by stoichiometric proportions of raw materials. Weighed mixtures of chemicals were homogenized by grinding with an agate mortar and pestle for 40 min, and calcined in alumina crucibles at 1000 °C for 36 h. They were then ground, pressed into pellets, and sintered at 1300 °C for 24 h in air followed by a furnace cooling. Each product was divided into two, of which one was post-annealed in oxygen ambient at 1000 °C for 3 h. Thus, the as-prepared and O_2-annealed samples were obtained.

Phase structure was verified by X-ray diffraction (XRD) using a Rigaku D/max 2550 V diffractometer with Cu Kα radiation. ^{57}Fe Mössbauer spectra were recorded in transmission mode on a constant acceleration spectrometer with a ^{57}Co(Pd) source. The velocity scale is calibrated periodically relative to α-Fe foil. Physically realistic fitting to the Mössbauer spectra was provided in terms of the sample structure and the ranges of isomer shifts (I.S.) and quadrupole splittings (Q.S.) reported for different Fe valences and occupational sites. Magnetic properties were measured using an HH-15 vibrating sample magnetometer (VSM) at room temperature. The iodometric titration was used to determine the total oxygen vacancy concentration (δ) in our samples. During the titration, the Ti^{4+} ions were deoxidized to Ti^{3+} and Fe^{3+} and Fe^{4+} were deoxidized to Fe^{2+}. Meanwhile the I^- ions were oxidized to I_2. The following reactions occurred:

$$B^{x+} + (x-2.3)\,I^- = B^{2.3+} + \frac{x-2.3}{2} I_2, \quad (1)$$

$$I_2 + 2S_2O_3^{2-} = 2I^- + S_4O_6^{2-}, \quad (2)$$

where B^{x+} expressed the B-site ions with the average valence x+ before the titration, and $B^{2.3+}$ expressed the B-site ions with the average valence 2.3+ after deoxidization by I^- ($B^{2.3+} = 0.3Ti^{3+} + 0.7Fe^{2+}$). The titration was carried out in the flowing N_2 gas to prevent the oxidization of I^- ions by air. From Eqs. (1) and (2) and the theorem of charge neutrality, the oxygen vacancy concentration can be calculated based on the amount of $Na_2S_2O_3$ consumed and the amount of sample applied.

3. Results and discussion

3.1. Effect of A-site K^+ substitution on microstructure and magnetic properties of as-prepared $Ba(Ti_{0.3}Fe_{0.7})O_3$

Fig. 1 shows the XRD patterns for $Ba(Ti_{0.3}Fe_{0.7})O_3$ samples with and without A-site K^+ substitution. The XRD data indicate no structural difference between two samples. All sharp diffraction peaks can be indexed to pure 6H-$BaTiO_3$ phase (JCPDS No. 34-0129). No evidence for any secondary phases such as K/Fe clusters or K/Fe oxides is found. Both samples are of single phase, crystallizing in a hexagonal perovskite structure. The K and Fe ions seem to have been incorporated into $BaTiO_3$ host lattice, replacing Ba^{2+} at the A site or Ti^{4+} at the B site. It is seen that the K^+ substitution at the A site of $Ba(Ti_{0.3}Fe_{0.7})O_3$ does not change phase composition or crystal structure.

Fig. 2 presents the magnetization versus magnetic field (M–H) curves for $Ba(Ti_{0.3}Fe_{0.7})O_3$ samples with and without A-site K^+ substitution. Room-temperature ferromagnetism is exhibited in $Ba(Ti_{0.3}Fe_{0.7})O_3$, indicated by a distinct hysteresis loop. A linear paramagnetic behavior superimposed upon hysteresis is also observed, originating from paramagnetic regions contained in the sample due to nearly isolated Fe ions, e.g., where the local Fe concentration is the lowest. Similar occurrences have been reported in other composition $Ba(Ti_{1-x}Fe_x)O_3$ [4,15,16] and $Ba(Ti_{0.65}M_{0.05}Fe_{0.3})O_3$ (M = Cr, Mn, Ni) ceramics [17]. The contributions from ferromagnetic and paramagnetic phases are separated according to the following equation:

$$M_T(H) = \frac{2M_S}{\pi} \tan^{-1}\left[\frac{H \pm H_C}{H_C} \tan\left(\frac{\pi S}{2}\right)\right] + N_g\mu\left[\mathrm{ctnh}\left(\frac{\mu H}{KT}\right) - \left(\frac{\mu H}{KT}\right)^{-1}\right], \quad (3)$$

where the first term is the usual function used to represent a ferromagnetic hysteresis curve, the second term is the usual expression for a paramagnetic component, M_S and $N_g\mu$ are the saturation magnetization of the ferromagnetic and paramagnetic parts, H_C is the coercivity, S is the squareness of the ferromagnetic loop, i.e., the ratio of the remanent magnetization, M_R, to M_S, and μ is the average moment [21,22]. It can be concluded from Fig. 2 that the saturation magnetization (M_S) of the ferromagnetic phase is about 0.0018 μ_B/Fe. On the contrary, paramagnetism is shown in $(Ba_{0.8}K_{0.2})(Ti_{0.3}Fe_{0.7})O_3$ at room temperature. The transition from ferromagnetism into paramagnetism suggests an obvious variation in magnetic exchange mechanism induced by A-site substitution of K^+.

In order to further investigate micro-configuration for clarifying the origin of magnetism, the valence state and occupational site of magnetic Fe ions were analyzed by Mössbauer spectroscopy, based on its high sensitivity to the Fe-atom surroundings. The Möss-

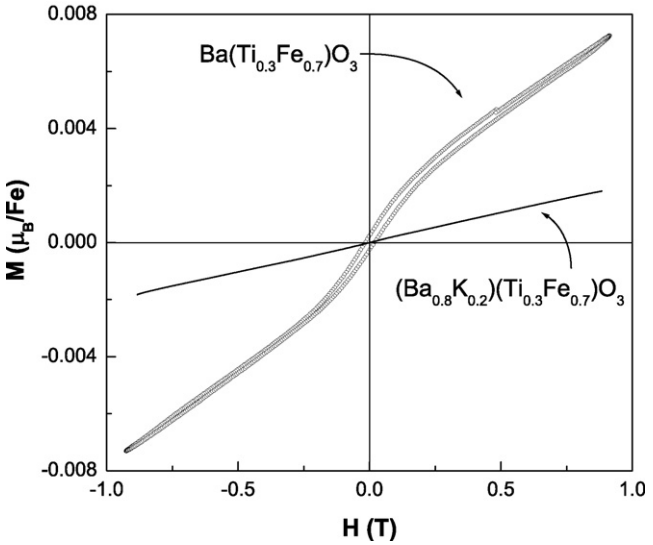

Fig. 2. Room-temperature M–H curves of $(Ba_{0.8}K_{0.2})(Ti_{0.3}Fe_{0.7})O_3$ and $Ba(Ti_{0.3}Fe_{0.7})O_3$ ceramics.

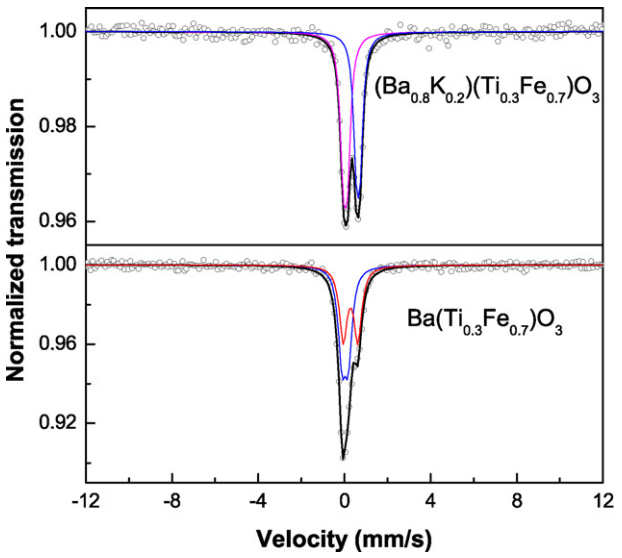

Fig. 3. Mössbauer spectra of $(Ba_{0.8}K_{0.2})(Ti_{0.3}Fe_{0.7})O_3$ and $Ba(Ti_{0.3}Fe_{0.7})O_3$ ceramics.

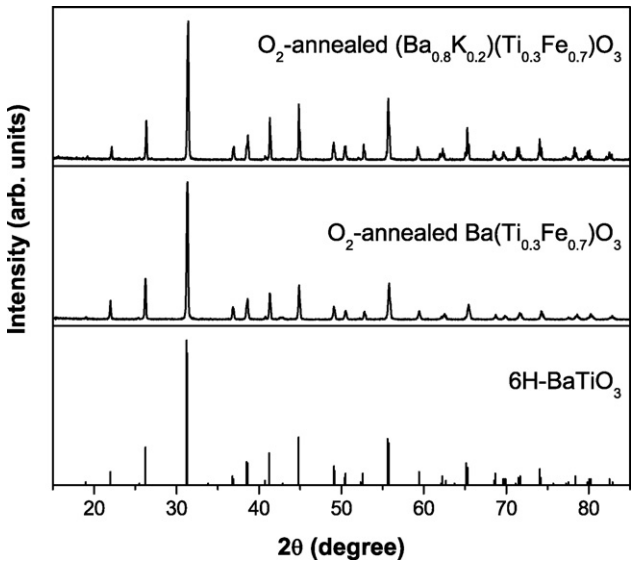

Fig. 4. XRD patterns of O_2-annealed $(Ba_{0.8}K_{0.2})(Ti_{0.3}Fe_{0.7})O_3$ and $Ba(Ti_{0.3}Fe_{0.7})O_3$ ceramics.

bauer results for $Ba(Ti_{0.3}Fe_{0.7})O_3$ samples with and without A-site K^+ substitution are given in Fig. 3 and Table 1. One can see that both spectra are composed of two overlapping doublets, without any sextet components caused by magnetically ordered phases in ferromagnetic $Ba(Ti_{0.3}Fe_{0.7})O_3$. This appears opposite to magnetization measurements, nevertheless similar phenomena have been observed in $Ti_{1-x}Fe_xO_2$ [21,23], $Zn_{1-x}Fe_xO$ [24,25], $Ba(Ti_{1-x}Fe_x)O_3$ [15,16] and $Ba(Ti_{0.65}M_{0.05}Fe_{0.3})O_3$ (M = Cr, Mn, Ni) [17]. The discrepancy may be explained by speculating that spin-lattice relaxation effects lead to a collapse of the Zeeman sextet of the magnetic component [15–17,21,23–25].

Taking into account I.S. and Q.S. [18,19,21,23,24,26,27], the presence of Fe^{2+} is ruled out based on the absence of absorption with higher velocity and larger splitting (an I.S. value of about 1.0 mm/s relative to α-Fe and a Q.S. value of about 2.0 mm/s would be expected, e.g. [21,23,24]) and the presence of Fe^{4+} (a negative I.S. value relative to α-Fe would be expected, e.g. −0.06 mm/s [26] and −0.01 mm/s [27]) is ruled out based on the I.S. values which all fall within the range for Fe^{3+}. The Fe ions are shown to be present in the form of Fe^{3+} in $Ba(Ti_{0.3}Fe_{0.7})O_3$, occupying pentahedral and octahedral Ti sites in the perovskite lattice. No indication is detected for impurity phases such as metallic Fe, Fe_3O_4 or γ-Fe_2O_3. Both XRD and Mössbauer results indicate the origin of measured magnetism from the intrinsic properties of sample. Our previous studies [17] showed that the room-temperature ferromagnetism of $Ba(Ti_{0.3}Fe_{0.7})O_3$ was produced by the competition between ferromagnetic pentahedral–octahedral Fe^{3+} super-exchange couplings mediated by the O^{2-} ions and anti-ferromagnetic pentahedral–pentahedral and octahedral–octahedral Fe^{3+} super-exchange couplings. In $(Ba_{0.8}K_{0.2})(Ti_{0.3}Fe_{0.7})O_3$, the Fe ions are present as Fe^{3+}, distributed over tetrahedral and octahedral Ti sites. The K^+ substitution at the A site induces changes not in Fe valence but in occupational site. The absence of pentahedral Ti site leads to the disappearance of ferromagnetic pentahedral–octahedral Fe^{3+} super-exchange interactions, while the super-exchange interactions of Fe^{3+} at tetrahedral and octahedral Ti sites bring about the ferromagnetism–paramagnetism transition.

Based on a half oxygen vacancy per pentahedral Ti site and one oxygen vacancy per tetrahedral Ti site [18,19], one can conclude from Table 1 that more oxygen vacancies have been formed to keep charge balance after introducing K^+, with a lower valence than Ba^{2+}, into the A site.

3.2. Effect of A-site K^+ substitution on microstructure and magnetic properties of O_2-annealed $Ba(Ti_{0.3}Fe_{0.7})O_3$

The XRD patterns for $(Ba_{0.8}K_{0.2})(Ti_{0.3}Fe_{0.7})O_3$ and $Ba(Ti_{0.3}Fe_{0.7})O_3$ samples annealed in O_2 are given in Fig. 4. As can be seen, the phase structure of two samples remains unchanged with annealing. Only the sharp peaks of 6H-$BaTiO_3$ are observed, indicating a hexagonal perovskite structure, and no impurities are detected. Combined with the XRD analysis in Section 3.1, it is concluded that A-site substitution of K^+ has no distinct influence on phase structure for both as-prepared and O_2-annealed $Ba(Ti_{0.3}Fe_{0.7})O_3$ samples.

Fig. 5 illustrates the M–H curves for $(Ba_{0.8}K_{0.2})(Ti_{0.3}Fe_{0.7})O_3$ and $Ba(Ti_{0.3}Fe_{0.7})O_3$ samples annealed in O_2. The $Ba(Ti_{0.3}Fe_{0.7})O_3$ sample still shows ferromagnetic ordering after O_2 annealing. From the M–H loop, the saturation magnetization is evaluated to be 0.0095 μ_B/Fe, over 5 times larger than that for the as-prepared state, indicating a beneficial effect of O_2 annealing on magnetization. Also, the coercivity (H_C) is significantly increased. For the $(Ba_{0.8}K_{0.2})(Ti_{0.3}Fe_{0.7})O_3$ sample, even more remarkable vari-

Table 1
Hyperfine parameters from Mössbauer spectra of $(Ba_{0.8}K_{0.2})(Ti_{0.3}Fe_{0.7})O_3$ and $Ba(Ti_{0.3}Fe_{0.7})O_3$ ceramics.

Samples	Subspectra	I.S. (mm/s)	Q.S. (mm/s)	Γ (mm/s)	Area (%)	Valence	Site
$(Ba_{0.8}K_{0.2})(Ti_{0.3}Fe_{0.7})O_3$	Doublet 1	0.04	0.20	0.17	53.6	Fe^{3+}	tetra-Ti
	Doublet 2	0.64	0.17	0.17	46.4	Fe^{3+}	octa-Ti
$Ba(Ti_{0.3}Fe_{0.7})O_3$	Doublet 3	0.28	0.67	0.20	47.6	Fe^{3+}	penta-Ti
	Doublet 4	0.03	0.30	0.20	52.4	Fe^{3+}	octa-Ti

Note: I.S., isomer shift (relative to α-Fe); Q.S., quadrupole splitting; Γ, Lorentzian line width; Area, relative area; tetra-Ti, tetrahedral Ti site; octa-Ti, octahedral Ti site; penta-Ti, pentahedral Ti site.

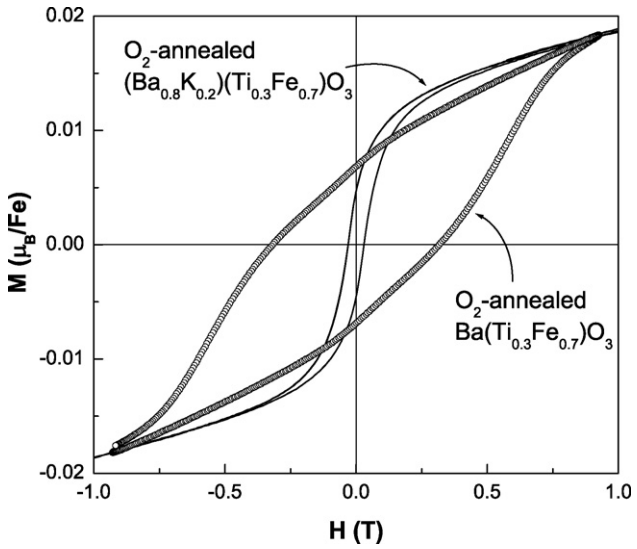

Fig. 5. Room-temperature M–H curves of O_2-annealed $(Ba_{0.8}K_{0.2})(Ti_{0.3}Fe_{0.7})O_3$ and $Ba(Ti_{0.3}Fe_{0.7})O_3$ ceramics.

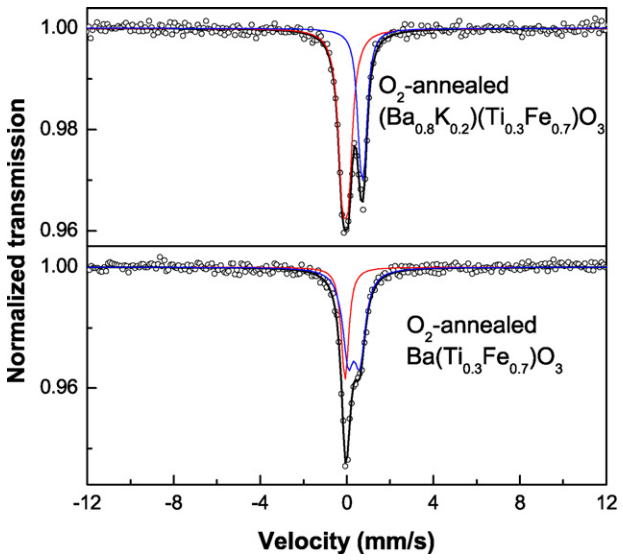

Fig. 6. Mössbauer spectra of O_2-annealed $(Ba_{0.8}K_{0.2})(Ti_{0.3}Fe_{0.7})O_3$ and $Ba(Ti_{0.3}Fe_{0.7})O_3$ ceramics.

ations have been observed after annealing in O_2, i.e. a transition from paramagnetism into ferromagnetism with the M_S value of 0.0123 μ_B/Fe. The evident difference in magnetism between the as-prepared and annealed states implies a great change in magnetic exchange mechanism during the process of O_2 annealing. Comparing two O_2-annealed samples, it is found that A-site substitution of K^+ can further improve the magnetic properties of annealed $Ba(Ti_{0.3}Fe_{0.7})O_3$, with an increase in M_S by 29.5% as well as a significant decrease in H_C.

For studying the dependence of Fe local environments in annealed $Ba(Ti_{0.3}Fe_{0.7})O_3$ on A-site K^+ substitution, the Mössbauer spectra were measured as presented in Fig. 6, and the corresponding hyperfine parameters are listed in Table 2. As is seen, the spectrum of annealed $Ba(Ti_{0.3}Fe_{0.7})O_3$ still comprises two doublets, but the hyperfine parameters obviously differ from those for the as-prepared state. During the O_2 annealing process, some of the Fe^{3+} ions are oxidized to a higher valence state, Fe^{4+}. At the same time oxygen vacancies are dramatically decreased, resulting in the approximate disappearance of pentahedral Ti site [18,19]. Combined with the I.S. and Q.S. values [18,19,21,23,24,26,27], therefore, the doublets (7) and (8) are respectively ascribed to Fe^{3+} and Fe^{4+}, distributed over octahedral Ti site in $BaTiO_3$ host lattice. Similarly, the Mössbauer spectrum of annealed $(Ba_{0.8}K_{0.2})(Ti_{0.3}Fe_{0.7})O_3$ also consists of two overlapping doublets. An unusual valence for iron, Fe^{4+}, is formed in the course of O_2 annealing, while tetrahedral Ti site is absent due to the decrease of oxygen vacancies. The doublets (5) and (6) are attributed to Fe^{3+} and Fe^{4+}, respectively, occupying octahedral Ti site.

Comparing the as-prepared state with the annealed one, the presence of Fe^{4+} and the variations in Fe occupational site after O_2 annealing are expected to be responsible for the remarkable changes of magnetic properties. In addition, the reduction of oxygen vacancies causes a decrease of the s-electron density at the Fe nucleus, leading to an increase in isomer shift of octahedral Fe^{3+} [28]. For $Ba(Ti_{0.3}Fe_{0.7})O_3$, the I.S. value is increased from 0.03 mm/s for the as-prepared state to 0.33 mm/s for the annealed state, while for $(Ba_{0.8}K_{0.2})(Ti_{0.3}Fe_{0.7})O_3$, the I.S. value is increased from 0.64 mm/s to 0.72 mm/s.

By comparison between $Ba(Ti_{0.3}Fe_{0.7})O_3$ and $(Ba_{0.8}K_{0.2})(Ti_{0.3}Fe_{0.7})O_3$, one can see that the introduction of K^+ into the A site induces an evident increase in I.S. value of octahedral Fe^{3+} for both as-prepared and annealed states. This may be related to the modification of Fe^{3+} local environments by A-site K^+ substitution. Another possible influencing factor is that there exist two types of octahedra in the crystal structure of 6H-$BaTiO_3$: $M1$ octahedron and $M2$ octahedron [19]. Moreover, it is found that non-isovalent substitution of K^+ at the A site facilitates the transformation of Fe^{3+} towards Fe^{4+} in the O_2 annealing process. The proportion of Fe^{4+} has been more than doubled, from 31.1% for annealed $Ba(Ti_{0.3}Fe_{0.7})O_3$ to 63.0% for annealed $(Ba_{0.8}K_{0.2})(Ti_{0.3}Fe_{0.7})O_3$. This can be explained by the further enhanced charge compensation mechanism due to the lower valence of K^+ than that of Ba^{2+}, besides by the effect of O_2 annealing.

As analyzed above, both XRD and Mössbauer measurements show O_2-annealed $Ba(Ti_{0.3}Fe_{0.7})O_3$ and $(Ba_{0.8}K_{0.2})(Ti_{0.3}Fe_{0.7})O_3$ to be monophasic 6H-$BaTiO_3$, with no evidence for any other phases involving combinations of Ba, K, Ti, Fe and O. Therefore, the room-temperature ferromagnetism observed is considered to be an intrinsic property of annealed samples. During the process of O_2 annealing, the Fe valence and occupational site are redistributed for two samples. The presence of a second valence for iron, Fe^{4+}, besides the usual one, Fe^{3+}, is observed, both occupying octahedral Ti site. The coexistence of Fe^{3+} and Fe^{4+} allows new magnetic exchange mechanism responsible for the ferromag-

Table 2
Hyperfine parameters from Mössbauer spectra of O_2-annealed $(Ba_{0.8}K_{0.2})(Ti_{0.3}Fe_{0.7})O_3$ and $Ba(Ti_{0.3}Fe_{0.7})O_3$ ceramics.

Samples	Subspectra	I.S. (mm/s)	Q.S. (mm/s)	Γ (mm/s)	Area (%)	Valence	Site
O_2-annealed $(Ba_{0.8}K_{0.2})(Ti_{0.3}Fe_{0.7})O_3$	Doublet 5	0.72	0.18	0.24	37.0	Fe^{3+}	octa-Ti
	Doublet 6	−0.07	0.28	0.24	63.0	Fe^{4+}	octa-Ti
O_2-annealed $Ba(Ti_{0.3}Fe_{0.7})O_3$	Doublet 7	0.33	0.54	0.19	68.9	Fe^{3+}	octa-Ti
	Doublet 8	−0.08	0.09	0.19	31.1	Fe^{4+}	octa-Ti

Note: I.S., isomer shift (relative to α-Fe); Q.S., quadrupole splitting; Γ, Lorentzian line width; Area, relative area; octa-Ti, octahedral Ti site.

Table 3
Comparison of some data for O_2-annealed $(Ba_{0.8}K_{0.2})(Ti_{0.3}Fe_{0.7})O_3$ and $Ba(Ti_{0.3}Fe_{0.7})O_3$ ceramics.

Samples	Fe^{4+} (%)	Fe^{4+} (/f.u.)	Fe^{4+}–Fe^{4+} (pairs/f.u.)	Fe^{3+}–Fe^{4+} (pairs/f.u.)	Fe^{3+}–Fe^{3+} (pairs/f.u.)	M_S (μ_B/Fe)
O_2-annealed $(Ba_{0.8}K_{0.2})(Ti_{0.3}Fe_{0.7})O_3$	63.0	0.4410	0.2205	0.2590	0.1295	0.0123
O_2-annealed $Ba(Ti_{0.3}Fe_{0.7})O_3$	31.1	0.2177	0.1089	0.2177	0.2412	0.0095

netic interactions in annealed samples. It is generally recognized that the Fe^{4+}–O^{2-}–Fe^{4+} interactions are ferromagnetic, while the Fe^{3+}–O^{2-}–Fe^{4+} and Fe^{3+}–O^{2-}–Fe^{3+} (octahedral–octahedral) interactions are anti-ferromagnetic [4,29–33]. The ferromagnetic Fe^{4+}–O^{2-}–Fe^{4+} super-exchange couplings dominate over the anti-ferromagnetic Fe^{3+}–O^{2-}–Fe^{4+} double-exchange and Fe^{3+}–O^{2-}–Fe^{3+} super-exchange couplings in the competition. This brings about a greatly increased saturation magnetization for $Ba(Ti_{0.3}Fe_{0.7})O_3$, and a paramagnetism–ferromagnetism transition for $(Ba_{0.8}K_{0.2})(Ti_{0.3}Fe_{0.7})O_3$.

Table 3 lists some data of two annealed samples for comparison. As can be seen, 31.1% of Fe^{3+} in $Ba(Ti_{0.3}Fe_{0.7})O_3$ is oxidized to a higher valence state, Fe^{4+}, during the course of O_2 annealing. New magnetic exchange mechanism increases the M_S value by a factor of over 5 times from 0.0018 μ_B/Fe for the as-prepared state to 0.0095 μ_B/Fe for the annealed state. After introducing K^+ into the A site, the charge compensation mechanism is further enhanced owing to a lower valence of K^+ than that of Ba^{2+}, making more Fe^{3+} ions (63.0%) be oxidized to Fe^{4+}. As listed in Table 3, the number of Fe^{4+}–Fe^{4+} pairs is increased with that of Fe^{4+} ions. This leads to a significant increase in ferromagnetic Fe^{4+}–O^{2-}–Fe^{4+} super-exchange as well as to a slight increase in anti-ferromagnetic Fe^{3+}–O^{2-}–Fe^{4+} double-exchange, but to an evident decrease in anti-ferromagnetic Fe^{3+}–O^{2-}–Fe^{3+} super-exchange. The competition finally gives rise to an enhanced magnetization with the M_S value 29.5% over that of annealed $Ba(Ti_{0.3}Fe_{0.7})O_3$ without A-site K^+ substitution. In addition, the H_C value for the annealed state is markedly reduced with introducing K^+ into the A site, which may be associated with the changes of sample composition, micro-configuration, morphology, etc. Further investigations are underway.

Since Mössbauer spectroscopy is sensitive to the surroundings of only Fe ions, oxygen vacancies, estimated based on a half oxygen vacancy per pentahedral Ti site and one oxygen vacancy per tetrahedral Ti site [18,19], are primarily those distributed around Fe. In order to obtain the total oxygen vacancy concentration (δ) in the samples more accurately, the conventional iodometric titration method was employed with the results listed in Table 4. The δ values calculated by iodometry are all higher than those estimated by the relation between oxygen vacancies and Ti sites. Besides, according to the Fe valence obtained from the Mössbauer spectra (Tables 1 and 2) and the theorem of charge neutrality, the oxygen vacancy concentration, denoted as δ', can also be calculated by assuming nominal contents and constant valences of 2+, 1+ and 4+ for Ba, K and Ti, respectively. The corresponding compositional formulas can be written as $Ba(Ti_{0.3}Fe^{3+}_{0.7})O_{3-0.35}$, $(Ba_{0.8}K_{0.2})(Ti_{0.3}Fe^{3+}_{0.7})O_{3-0.45}$, $Ba(Ti_{0.3}Fe^{3+}_{0.4823}Fe^{4+}_{0.2177})O_{3-0.24115}$ and $(Ba_{0.8}K_{0.2})(Ti_{0.3}Fe^{3+}_{0.259}Fe^{4+}_{0.441})O_{3-0.2295}$, respectively, for as-prepared $Ba(Ti_{0.3}Fe_{0.7})O_3$ and $(Ba_{0.8}K_{0.2})(Ti_{0.3}Fe_{0.7})O_3$ and annealed $Ba(Ti_{0.3}Fe_{0.7})O_3$ and $(Ba_{0.8}K_{0.2})(Ti_{0.3}Fe_{0.7})O_3$. The obtained δ' values are also shown in Table 4 for comparison. One can see that the values of δ' are consistent with those of δ within the limits of error. For the as-prepared samples, the number of oxygen vacancies is increased with A-site substitution of K^+. Upon annealing in O_2, oxygen vacancies are decreased remarkably. These results are in good agreement with the former analyses and give further support to the discussions about magnetic exchange mechanism.

Table 4
The oxygen vacancy concentrations δ (calculated by iodometry) and δ' (calculated by the theorem of charge neutrality based on the Fe valence obtained from Mössbauer spectroscopy).

Samples	δ (f.u.$^{-1}$)	δ' (f.u.$^{-1}$)
As-prepared $Ba(Ti_{0.3}Fe_{0.7})O_3$	0.354	0.35
As-prepared $(Ba_{0.8}K_{0.2})(Ti_{0.3}Fe_{0.7})O_3$	0.456	0.45
O_2-annealed $Ba(Ti_{0.3}Fe_{0.7})O_3$	0.240	0.24115
O_2-annealed $(Ba_{0.8}K_{0.2})(Ti_{0.3}Fe_{0.7})O_3$	0.233	0.2295

In addition, Sundaresan et al. [34] reported that ferromagnetism occurred in nanoparticles of nonmagnetic oxides such as CeO_2, Al_2O_3, ZnO, In_2O_3 and SnO_2. And a recent work [35] showed room-temperature ferromagnetism in non-doped nanocrystalline specimens of $BaTiO_3$. For our samples, the average grain sizes of as-prepared $Ba(Ti_{0.3}Fe_{0.7})O_3$ and $(Ba_{0.8}K_{0.2})(Ti_{0.3}Fe_{0.7})O_3$ and annealed $Ba(Ti_{0.3}Fe_{0.7})O_3$ and $(Ba_{0.8}K_{0.2})(Ti_{0.3}Fe_{0.7})O_3$ estimated by the Scherrer formula are 46.3, 45.9, 50.3 and 53.6 nm, respectively. Although these four samples are all nanometer-sized, we can rule out the possibility of the origin of ferromagnetism from oxygen vacancies at the surface of nanoparticles. If such a nanoscale effect were responsible for the ferromagnetism measured in as-prepared $Ba(Ti_{0.3}Fe_{0.7})O_3$ and annealed $Ba(Ti_{0.3}Fe_{0.7})O_3$ and $(Ba_{0.8}K_{0.2})(Ti_{0.3}Fe_{0.7})O_3$, the as-prepared $(Ba_{0.8}K_{0.2})(Ti_{0.3}Fe_{0.7})O_3$ sample (45.9 nm) should also be ferromagnetic at room temperature and the saturation magnetization would be decreased with the increasing grain size after annealing. Instead, the opposite behaviors are observed in the magnetic measurements. Therefore we attribute the magnetism of our samples to the exchange interactions between the Fe ions with different Ti sites and valence states.

4. Conclusions

$(Ba_{0.8}K_{0.2})(Ti_{0.3}Fe_{0.7})O_3$ and $Ba(Ti_{0.3}Fe_{0.7})O_3$ ceramics were synthesized using the solid-state reaction method, and subsequently annealed in oxygen. The results show that all as-prepared and annealed samples are of a single 6H-$BaTiO_3$ hexagonal perovskite phase with the K and Fe ions dissolved into the matrix replacing A-site Ba^{2+} and B-site Ti^{4+}, respectively. For as-prepared samples, the introduction of K^+ into the A site does not change Fe valence of 3+ but Fe occupational distribution from pentahedral/octahedral to tetrahedral/octahedral Ti sites. The resulting disappearance of ferromagnetic pentahedral–octahedral Fe^{3+} super-exchange interactions allows $(Ba_{0.8}K_{0.2})(Ti_{0.3}Fe_{0.7})O_3$ to exhibit paramagnetism originating from the super-exchange interactions of Fe^{3+} at tetrahedral and octahedral Ti sites. As for O_2-annealed samples, the Fe^{3+} and Fe^{4+} ions coexist, occupying octahedral Ti site. The ferromagnetic Fe^{4+}–O^{2-}–Fe^{4+} super-exchange interactions induce a remarkably increased saturation magnetization by more than 5 times in $Ba(Ti_{0.3}Fe_{0.7})O_3$, and even a paramagnetism–ferromagnetism transition in $(Ba_{0.8}K_{0.2})(Ti_{0.3}Fe_{0.7})O_3$. In the annealed state, non-isovalent A-site substitution of K^+ facilitates the charge compensation mechanism and therefore the oxidation of Fe^{3+} to Fe^{4+}

during the O_2 annealing process, producing a further enhanced saturation magnetization for annealed $(Ba_{0.8}K_{0.2})(Ti_{0.3}Fe_{0.7})O_3$, 29.5% higher than that of annealed $Ba(Ti_{0.3}Fe_{0.7})O_3$.

Acknowledgements

The authors would like to acknowledge financial assistances from "Chen Guang" project supported by Shanghai Municipal Education Commission and Shanghai Education Development Foundation (No. 09CG45), from Shanghai Normal University (No. SK200944), and from Leading Academic Discipline Project of Shanghai Normal University (No. DZL712).

References

[1] H. Nakayama, H. Katayama-Yoshida, Jpn. J. Appl. Phys. 40 (2001) L1355.
[2] J.S. Lee, Z.G. Khim, Y.D. Park, D.P. Norton, N.A. Theodoropoulou, A.F. Hebard, J.D. Budai, L.A. Boatner, S.J. Pearton, R.G. Wilson, Solid-State Electron. 47 (2003) 2225.
[3] R. Maier, J.L. Cohn, J.J. Neumeier, L.A. Bendersky, Appl. Phys. Lett. 78 (2001) 2536.
[4] R. Maier, J.L. Cohn, J. Appl. Phys. 92 (2002) 5429.
[5] A. Rajamani, G.F. Dionne, D. Bono, C.A. Ross, J. Appl. Phys. 98 (2005) 063907.
[6] O. Peña, M. Bahout, D. Gutiérrez, J.F. Fernández, P. Durán, C. Moure, J. Phys. Chem. Solids 61 (2000) 2019.
[7] D. Gutiérrez, O. Peña, K. Ghanimi, P. Durán, C. Moure, J. Phys. Chem. Solids 63 (2002) 1975.
[8] M. Mouallem-Bahout, T. Roisnel, G. André, D. Gutierrez, C. Moure, O. Peña, Solid State Commun. 129 (2004) 255.
[9] M. Mouallem-Bahout, T. Roisnel, G. André, C. Moure, O. Peña, J. Solid State Chem. 180 (2007) 1737.
[10] F.Z. Huang, X.M. Lu, W.W. Lin, X.M. Wu, Y. Kan, J.S. Zhu, Appl. Phys. Lett. 89 (2006) 242914.
[11] M. Fiebig, J. Phys. D 38 (2005) R123.
[12] Y. Ohno, D.K. Young, B. Beschoten, F. Matsukura, H. Ohno, D.D. Awshalom, Nature (London) 402 (1999) 790.
[13] M. Fiebig, Th. Lottermoser, D. Fröhlich, A.V. Goltsev, R.V. Pisarev, Nature (London) 419 (2002) 818.
[14] N.A. Hill, J. Phys. Chem. B 104 (2000) 6694.
[15] F.T. Lin, D.M. Jiang, X.M. Ma, W.Z. Shi, J. Magn. Magn. Mater. 320 (2008) 691.
[16] F.T. Lin, D.M. Jiang, X.M. Ma, W.Z. Shi, Physica B 403 (2008) 2525.
[17] F.T. Lin, W.Z. Shi, J. Alloys Compd. 475 (2009) 64.
[18] C.A. McCammon, A.I. Becerro, F. Langenhorst, R.J. Angel, S. Marion, F. Seifert, J. Phys.: Condens. Matter 12 (2000) 2969.
[19] E. Mashkina, C. McCammon, F. Seifert, J. Solid State Chem. 177 (2004) 262.
[20] R.D. Shannon, Acta Crystallogr., Sect. A: Cryst. Phys., Diffr., Theor. Gen. Crystallogr. 32 (1976) 751.
[21] X.Y. Pan, D.M. Jiang, Y. Lin, X.M. Ma, J. Magn. Magn. Mater. 305 (2006) 388.
[22] M.B. Stearns, Y. Cheng, J. Appl. Phys. 75 (1994) 6894.
[23] F. Lin, D.M. Jiang, Y. Lin, X.M. Ma, Physica B 403 (2008) 2193.
[24] Y. Lin, D.M. Jiang, F. Lin, W.Z. Shi, X.M. Ma, J. Alloys Compd. 436 (2007) 30.
[25] G.Y. Ahn, S.-I. Park, I.-B. Shim, C.S. Kim, J. Magn. Magn. Mater. 282 (2004) 166.
[26] P.K. Gallagher, J.B. MacChesney, D.N.E. Buchanan, J. Chem. Phys. 43 (1965) 516.
[27] A. Hero, U. Gonser, H. Engelmann, H.J. Hagemann, Ferroelectrics 65 (1985) 211.
[28] F.S. Li, L. Wang, J.B. Wang, Q.G. Zhou, X.Z. Zhou, H.P. Kunkel, G. Williams, J. Magn. Magn. Mater. 268 (2004) 332.
[29] T. Matsui, E. Taketani, N. Fujimura, T. Ito, K. Morii, J. Appl. Phys. 93 (2003) 6993.
[30] J.B. Goodenough, A. Wold, R.J. Arnott, N. Menyuk, Phys. Rev. 124 (1961) 373.
[31] S. Mori, J. Phys. Soc. Jpn. 28 (1970) 44.
[32] G.F. Dionne, J. Appl. Phys. 79 (1996) 5172.
[33] T. Matsui, H. Tanaka, N. Fujimura, T. Ito, H. Mabuchi, K. Morii, Appl. Phys. Lett. 81 (2002) 2764.
[34] A. Sundaresan, R. Bhargavi, N. Rangarajan, U. Siddesh, C.N.R. Rao, Phys. Rev. B 74 (2006) 161306.
[35] R.V.K. Mangalam, N. Ray, U.V. Waghmare, A. Sundaresan, C.N.R. Rao, Solid State Commun. 149 (2009) 1.